SSRG International Journal of Electrical and Electronics Engineering
ISSN: 2348-8379/ https://doi.org/10.14445/23488379/IJEEE-V13I8P112

Volume 13 Issue 8, 141-153, August 2026

Original Article

Gain-Bandwidth Trade-off Reduction in an H-Shaped Dielectric Resonator Antenna Using Coplanar Substrate Integrated Waveguide Feeding for 5G Application

Hajar Ja'afar[1,3*], Rina Abdullah[2,3], Mohd Haizal Jamaluddin[4], Hizamel M. Hizan[5,] Rabiatuladawiah Akhbar[2,6]

[1]*Faculty of Electrical Engineering, Pasir Gudang, Universiti Teknologi MARA, 81750 Masai, Johor, Malaysia.*
[2]*Faculty of Electrical Engineering, Terengganu, Universiti Teknologi MARA, 23000 Dungun, Terengganu, Malaysia.*
[3]*Antenna Research Centre, Faculty of Electrical Engineering, Universiti Teknologi MARA,40450 Selangor, Malaysia.*
[4]*Wireless Communication Center, Faculty of Electrical Engineering, Universiti Teknologi Malaysia, 81310, Malaysia.*
[5]*Centre for Intelligent Network TM Research & Development Cyberjaya,63000 Cyberjaya, Selangor, Malaysia.*
[6]*Centre of Foundation Studies, Universiti Teknologi MARA, 43800 Dengkil, Selangor, Malaysia.*

[*]*Corresponding Author: hajarj422@uitm.edu.my*

Received: 08 June 2026 Revised: 20 July 2026 Accepted: 10 August 2026 Published: 25 August 2026

Abstract - *Due to the simplicity of the geometry, Rectangular Dielectric Resonator Antennas (RDRAs) are widely used, and they provide more flexibility in controlling the resonant frequency by varying the length, width, and height of the antenna. The traditional RDRAs, however, usually have a trade-off between gain and impedance bandwidth, and it is difficult to enhance both parameters simultaneously. Such a gain–bandwidth trade-off is a key issue in antenna design, particularly for new 5G wireless communication systems that require high gain and wide bandwidth with a compact antenna profile. To solve this problem, this paper introduces an improved design method for reducing the gain-bandwidth trade-off based on the combination of the CP-SIW feeding mechanism and an optimized H-shaped dielectric resonator structure. In this study, the antenna was excited using a Coplanar Substrate-Integrated Waveguide (CP-SIW) feeding mechanism with a modified resonator geometry. The CP-SIW feed contributed to the improvement in antenna gain, while the impedance bandwidth was enhanced through the transformation of the conventional RDRAs into an H-shaped resonator configuration. The antenna was fabricated on a Rogers RT/Duroid 5880 substrate (εr = 2.2) with a thickness of 1.57 mm. The dielectric resonator was made of ceramic material with a relative permittivity of 15, while the modified H-shaped structure was studied using an effective permittivity model, considering the dielectric, substrate, and air regions. The simulated results showed a clear improvement in performance, where the impedance bandwidth increased from 10.3% for the conventional RDRA to 13.9% for the proposed H-shaped Dielectric Resonator Antenna (H-DRA). In addition, the antenna gain significantly improved from 3.92 dBi (without SIW integration) to 9.3 dBi with the CP-SIW feed, and slightly decreased to 9.14 dBi after implementing the optimized H-DRA configuration. The radiation efficiency did not fall below 98%, which is considered excellent energy efficiency. The measured results are also presented to further validate the simulation results, in which the fabricated prototype was found to have a measured bandwidth of 27.7% and a peak gain of 8.29 dBi. The simulated results suggest good agreement with the measured results, which confirms the validity of the proposed design. Overall, the proposed CP-SIW-fed H-shaped DRA offers a promising solution for reducing the gain–bandwidth trade-off in high-performance 5G wireless communication applications.*

Keywords - *H Shaped DRA, CP-SIW Feed, Gain-Bandwidth Trade-off, Bandwidth Enhancement, Sub 6 GHz.*

1. Introduction

Research on Substrate Integrated Waveguide (SIW) integrated Dielectric Resonator Antenna (DRA) has received increasing attention, particularly for 5G wireless communication systems [1-4]. One of the main motivations is the need for antenna solutions capable of supporting the high data rates, low latency, and compact device requirements of modern wireless systems. Several studies have demonstrated that SIW-integrated DRA designs can meet important antenna performance requirements for current 5G applications [5-7]. DRAs are generally characterized by high radiation efficiency, low dielectric loss, and compact size, whereas SIW technology provides a low-profile, low loss planar waveguiding platform that can be readily integrated with other microwave components[8, 9]. These complementary characteristics make SIW integrated DRA designs an attractive solution for developing compact and efficient antennas for 5G systems.

Consequently, SIW integrated DRA designs have been extensively investigated for both Sub 6 GHz and millimeter wave 5G applications because of their capability to improve antenna gain, impedance bandwidth, and radiation performance. Despite these advantages, existing SIW integrated DRA designs still exhibit several limitations that restrict their implementation in high performance 5G systems. A common observation in the literature is that high gain SIW integrated DRA designs generally exhibit impedance bandwidths below 10% [1, 3, 5, 10]. Conversely, recent studies have reported wideband SIW integrated DRA designs for millimeter wave applications [11, 12].

However, improving the impedance bandwidth often leads to a reduction in antenna gain, reflecting the inherent gain bandwidth trade-off in SIW integrated DRA designs. Furthermore, SIW integration introduces additional challenges related to mode excitation, gain stabilization, bandwidth control, and fabrication accuracy.

Therefore, despite the substantial progress reported in the literature, achieving high gain and wide impedance bandwidth simultaneously remains a major challenge for SIW integrated DRA designs. These limitations highlight the need for improved antenna configurations capable of reducing the inherent gain bandwidth trade-off while satisfying the performance requirements of Sub-6 GHz 5G systems.

To address these limitations, this work proposes a CP-SIW integrated rectangular DRA operating at 3.5 GHz. The CP-SIW feeding structure is employed to enhance the antenna gain, while the conventional rectangular resonator is modified into an H-shaped configuration to improve the impedance bandwidth without degrading the gain performance achieved by the CP-SIW integration.

The modified H-shaped resonator enhances the electromagnetic coupling between the resonator and the CP-SIW feed, promoting stronger mode excitation and a wider operating bandwidth while maintaining the high gain performance achieved through CP-SIW integration. The proposed antenna is validated through both simulation and experimental measurement, and its performance is evaluated in terms of impedance bandwidth, antenna gain, and radiation characteristics.

This work addresses the limitations of existing SIW integrated DRA designs by combining CP-SIW integration structure with a modified H-shaped resonator to simultaneously enhance antenna gain and impedance bandwidth. Consequently, the proposed antenna reduces the inherent gain bandwidth trade-off while satisfying the performance requirements of Sub 6 GHz 5G applications. The antenna performance was initially evaluated through numerical simulations and then validated experimentally using the fabricated prototype.

2. Literature Review

2.1. High Gain SIW Integrated DRA Designs and Bandwidth Limitation

Numerous SIW integrated DRA designs have been proposed to enhance antenna gain for high performance wireless communication systems. Various techniques, including stacked resonators, parasitic arrays, and impedance matching structures, have been investigated to improve antenna gain and radiation performance. For instance, Sahu et al.[3] designed and analyzed a stacked SIW fed DRA with hemispherical, spherical, and frustum-shaped resonators for a measured gain of 8.4 dBi. However, the antenna exhibited a relatively narrow impedance bandwidth of only 4.64%. To further improve gain, Abdel Wahab et al. [13] fabricated a parasitic SIW-DRA array configuration, where parasitic dielectric resonators were positioned near the driven element. The measured gain increased to 12 dBi, while the impedance bandwidth remained limited to approximately 8.9%.

Although the parasitic configuration significantly improved antenna gain, the impedance bandwidth remained below 10%, indicating that gain enhancement alone is insufficient to achieve a wide impedance bandwidth. Despite the improvement, the antenna structure becomes more complex. In another study, Chemweno et al. [5] employed inductive shorting vias and a Defected-Ground Structure (DGS) to improve the impedance matching characteristics of an SIW fed DRA operating in the D band.

Their design achieved a gain of 8.79 dBi with an impedance bandwidth of 9%. Similarly, impedance-matching techniques improved gain performance, however, only marginal bandwidth improvement was achieved. Overall, existing high gain SIW integrated DRA designs have primarily relied on stacked resonators, parasitic elements, and impedance matching techniques to improve antenna gain. Nevertheless, most reported designs still exhibit impedance bandwidths below 10%, indicating that achieving wider impedance bandwidth while maintaining high antenna gain remains a significant challenge.

2.2. Wideband SIW Integrated DRA Designs and Gain Reduction

Several studies have been conducted to increase the impedance bandwidth of a DRA fed by an SIW. Luo et al. [6] presented a wideband fractal rectangular dielectric resonator antenna with the SIW feeding and hook shaped electric dipole. The antenna's measured impedance bandwidth was 19.5% based on a Koch-like fractal geometry and dual mode excitation, and the average gain of the antenna was 5.96 dBi. Although the fractal geometry successfully broadened the impedance bandwidth to 19.5%, the measured gain was limited to 5.96 dBi, indicating that bandwidth enhancement alone does not necessarily provide high gain performance. A cylindrical dielectric resonator antenna with a perforated feed structure was proposed by Rahmati et al. [14]. The antenna had an impedance bandwidth of 18.5% and a maximum gain of 8.6 dBi, which were obtained with the use of perforation and excitation of higher-order modes. The proposed design achieved a measured bandwidth of 28.7% with a gain of 8.1 dBi. Similarly, perforation and higher order mode excitation further improved the impedance bandwidth, however, the antenna gain remained below 9 dBi despite the wider operating bandwidth.

Overall, existing wideband SIW integrated DRA designs primarily rely on fractal geometries, perforation techniques, and higher order mode excitation to broaden the impedance bandwidth.

Nevertheless, these approaches generally provide only moderate antenna gain or require increasingly complex antenna structures. These observations indicate that simultaneously achieving a wide impedance bandwidth and high antenna gain remains a significant challenge in SIW integrated DRA designs, motivating a comparative evaluation of existing approaches to identify the remaining research gap.

2.3. Comparative Analysis and Research Gap

Table 1 summarizes the performance comparison of representative SIW-integrated DRA designs reported in the literature. As shown in Table 1, high gain SIW-integrated DRA designs (>8 dBi), such as those reported in [3, 13] and [5], generally exhibit impedance bandwidth below than 10%. In contrast, wideband SIW integrated DRA designs reported in [6, 14] achieve impedance bandwidths exceeding 18%, however, these designs provide only moderate antenna gain or require more complex antenna configurations. These comparisons indicate that simultaneously achieving wide impedance bandwidth and high antenna gain in a single SIW integrated DRA design remains a significant challenge. Therefore, there remains a need for an SIW integrated DRA design capable of simultaneously achieving a wide impedance bandwidth and high antenna gain without introducing excessive structural complexity. To address this research gap, the proposed work integrates a CP-SIW feeding structure with an H-shaped dielectric resonator to reduce the inherent gain bandwidth trade-off through simultaneous feed and resonator optimization.

Table 1. Comparison of representative SIW-DRA designs in terms of gain, impedance bandwidth, design complexity, and validation method.

Ref	Technique	Gain (dBi)	FBW (%)	Complexity	Validation
[3]	Stacked SIW-DRA	8.4	4.64	High	Measurement
[13]	SIW fed Parasitic DRA Array	12.0	8.9	High	Measurement
[5]	Shorting Vias + DGS	8.79	9.0	Moderate	Simulation
[6]	Fractal SIW-DRA	5.96	19.5	High	Measurement
[14]	Perforated SIW-DRA	8.6	18.5	Moderate to High	Simulation
Proposed Work	CP-SIW fed H-shaped DRA	8.29	27.7	Low to Moderate	Measurement
*Complexity is qualitatively assessed based on antenna structural complexity, additional resonator elements, and fabrication requirements.					

3. Research Method

In the present research, the effect of the feeding structure and modified resonator shape on the gain and bandwidth of an SIW fed DRA is investigated. This is a general approach that has three main components. First, the design and analysis of RDRA with various planar feeding mechanisms were performed. Second, the resonator's structural modification was used to enhance the resonator's impedance bandwidth, thus improving the coupling efficiency.

Third, full-wave simulation and experimental validation were conducted to evaluate the electromagnetic performance of the antenna. The basic radiator chosen was the RDRA due to its simple geometry for easier analysis and better control of resonant modes than other DRA shapes [15]. Standard theoretical procedures were performed to plan the baseline RDRA for the first stage, and the RDRA was analyzed for three different planar feeding lines to determine which would be the best way to excite the RDRA. After that, the RDRA geometry was changed, and its influence on the performance of the bandwidth was studied. CST Microwave Studio (CST MWS®) was used for all the antenna designs and simulations, antenna optimization and parametric analysis were carried out to perform full wave electromagnetic modeling accurately during the development process.

3.1. Rectangular DRA

In this study, a single-element RDRA was designed and installed on the Rogers type 5880 substrate (as shown in Figure 1). The antenna was designed for the desired resonant frequency of 3.5 GHz. The fundamental resonant frequency (f_0) of the RDRA was obtained using the Dielectric Waveguide Model (DWM) [16]. This equation gives a basic analytical framework as a tool to predict the resonant frequencies of different mode numbers, and it is also a good approximation to estimate the modes of high-permittivity dielectric resonators.

Figure 1 represents a basic single RDRA with specific dimensions (length x width x height), which represent a, b, and h (28 mm × 32 mm × 26 mm), respectively. The RDRA used a dielectric material that has a relative permittivity of 15. It was positioned above a 0.035 mm-thick copper layer supported by a 1.57 mm-thick Rogers 5880 substrate. The substrate has a dielectric constant of 2.2 and provides physical support for the antenna structure while contributing to its electromagnetic behaviour. Both the ground plane and the substrate shared identical lateral dimensions of 56 mm × 56 mm × 1.57 mm.

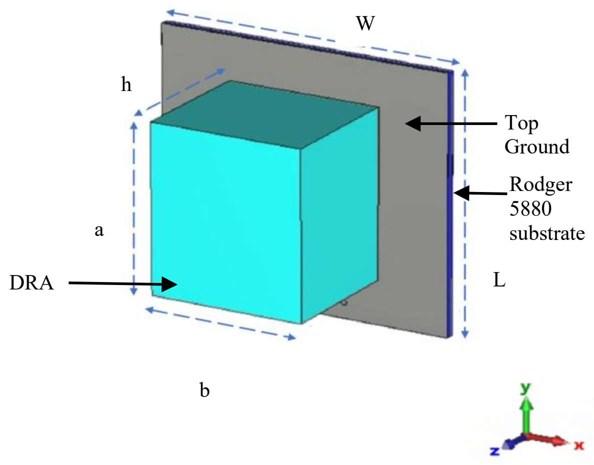

Fig. 1 The basic design of a single RDRA

The theoretical modal behavior of the RDRA is described by the characteristic equations shown in (1)–(3), where k_x, k_y, k_z, and k_0 represent the wavenumbers in the rectangular dielectric volume. Based on these expressions, the dominant mode can be estimated, and an approximation for the resonator's optimal size for operation at a certain frequency can be given. The design parameter values for the baseline RDRA are summarized in Table 2.

$$k_y \tan(k_y W_d/2) = \sqrt{(\varepsilon_{rd} - 1)k_0^{\,2} - k_y^{\,2}} \tag{1}$$

$$k_x^{\,2} + k_y^{\,2} + k_z^{\,2} = \varepsilon_{rd}\, k_0^{\,2} \tag{2}$$

$$k_x = \frac{\pi}{L_d}, \quad k_z = \frac{\pi}{2H_d}, \qquad k_0 = \frac{2\pi f0}{c} \tag{3}$$

Table 2. Dimension of basic RDRA

Dimension	Symbol	Value (mm)
Length of DR	a	28
Width of DR	b	32
Height of DR	h	26
Length of substrate	L_{sub}	56
Width of substrate	W_{sub}	56
Height of substrate	h_{sub}	1.57

3.2. Basic Antenna Planar Feeding Lines

The RDRA antenna was analyzed using three different planar feeding lines to determine the optimal design for enhanced performance. A planar feeding structure refers to a mechanism that delivers power to the antenna through planar geometries, either embedded within the substrate or positioned on the same layer as the resonating element. In this work, three commonly used planar feeding techniques, Microstrip Line (ML), Aperture-Coupled (AC) feed, and Coplanar Waveguide (CPW), were implemented for the single RDRA, as illustrated in Figure 2.

One of the popular techniques of antenna design is the ML feed. This is a conducting strip printed on a dielectric substrate with a ground plane on the back. A simple structure such as this enables the delivery of power to the antenna with relatively low loss. In this work, an ML feed with dimensions of 4.6 mm × 28 mm was used to excite the RDRA, which was mounted on an RT Rogers 5880 substrate, as shown in Figure 2(a). The AC feed is an indirect feeding approach frequently applied in both microstrip and DRAs. Energy was transferred through a small slot cut in the ground plane, allowing the radiating element to be excited through electromagnetic coupling. The AC feed used in this study has dimensions of 4.6 mm × 28 mm and was implemented on the RT5880 substrate, as illustrated in Figure 2(b).

The CPW feed, however, is composed of a single conducting strip surrounded by two ground planes on the same side of the dielectric substrate, as opposed to ML and AC. The return paths are provided by the outermost ground planes, and the signal is provided in the center strip. The characteristic impedance (usually 50 Ω) is determined by the signal strip width and the distance between the signal strip and the ground planes. CPW provides good electromagnetic confinement around the conductor and can be used for high-frequency and wideband operation. In this work, the dimensions of CPW were 4.05 mm × 36 mm, and the configuration can be seen in Figure 2(c).

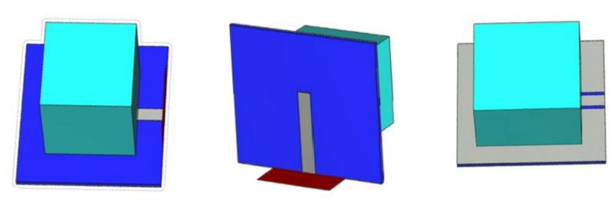

(a) (b) (c)

Fig. 2 Three feeding lines for the single RDRA (a) ML, (b) Aperture coupler, and (c) CPW.

3.3. Integrated with Substrate Integrated Waveguide

The SIW was based on the conventional Rectangular Waveguide (RWG) [18, 19] and the Dielectric-Filled Waveguide (DFW). Although introduced in a planar, substrate-based configuration, the propagation and dispersion of the SIW are similar to those of a conventional RWG. This behavior is due to its construction, where the metalized via holes form two parallel rows that simulate the sidewalls of a rectangular waveguide, as shown in Figure 3.

As for modal behavior, the SIW primarily supports TEm0 modes for guided-wave propagation, whereas other higher-order modes, including TMmn modes, may experience significant leakage if excited [17].

The metalized vias provide conductive paths from the top to the bottom metal, which disrupt the longitudinal surface-current distributions needed for TM mode propagation and cause the modes to radiate away instead of being sustained. On the contrary, for TE modes, the current distribution is continuous along the via rows, which allows the currents to be efficiently confined and propagated.

At the same time, it permits low-loss propagation in the SIW structure. The fundamental design parameters [18] of an SIW structure include the via diameter (D), via pitch (S), and the SIW width (Wsiw). In practice, the SIW width is typically smaller than the width of a conventional rectangular waveguide due to the existence of the dielectric substrate.

The parameter Wd denotes the corresponding width of the Dielectric-Filled Waveguide (DFW). These parameters are related to the equivalent rectangular waveguide width (W) and the dielectric-filled waveguide width (Wd), as defined by the expressions in (4)–(8). Equation (4) estimates the cut off frequency of the dominant TE10 mode, while Equation (5) gives the width of an equivalent dielectric-filled waveguide used to determine the effective SIW width. Equation (6) relates the actual SIW width to its equivalent DFW width, accounting for the discontinuity introduced by the via posts.

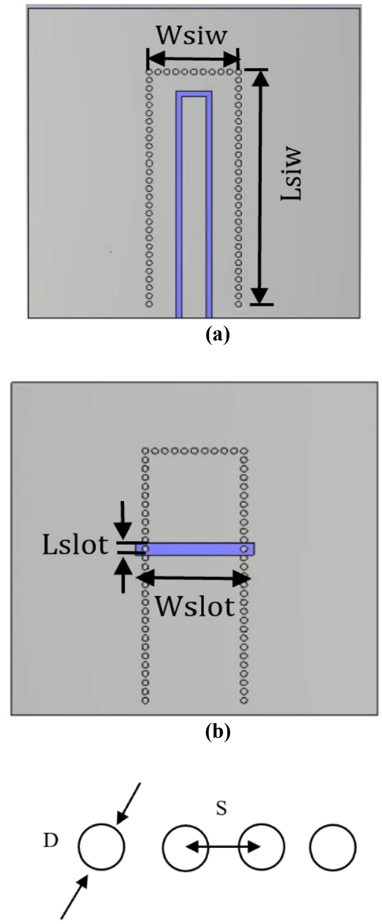

(c)
Fig. 3 Structural configuration of the SIW, (a) SIW width and length parameters (Wsiw, Lsiw), (b) Coupling slot dimensions (Wslot, Lslot), and (c) Metalized via parameters showing via diameter, (d) Spacing (S).

Table 3. Dimension of SIW

Dimension	Symbol	Value (mm)	Dimension	Symbol	Value (mm)
Width of SIW	W_{siw}	15	Length of slot	L_{slot}	2
Length of SIW	L_{siw}	42	Diameter of via	D	1
Length of slot	W_{slot}	16	Spacing of vias	S	1.5

All SIW dimensions used in this study, including the SIW width, slot dimensions, via diameter, and via spacing, are summarized in Table 3.

These mathematical expressions collectively ensure an accurate SIW design and reliable propagation behavior when the configuration is integrated with the RDRA.

Proper selection of D, S, and Wsiw can make the SIW behave very similarly to a conventional waveguide, while also taking advantage of the compact and planar integration of substrate-based technologies.

These planar feeding structures presented in the previous section are then combined with an SIW to enhance the feeding network's coupling efficiency and lower radiation loss in the RDRA feeding network.

cutoff frequency, $f_c = c/2W$ (4)

DFW width $W_d = W/\sqrt{\varepsilon_r}$ (5)

SIW width or center-to-center distance $W_{siw} = W_d + D^2/0.95$ (6)

The conditions required for SIW; $S \leq 2D$ and $D < \lambda_g/5$ (7)

Guided wavelength; $\lambda_{gsiw} = \frac{\lambda_0}{\sqrt{\varepsilon_r[1-(\frac{f_c}{f_0})^n]}}$; $\lambda_0 = c/f_0$ (8)

Where ; λ_0 is the free space wavelength,
f_c is the cutoff frequency,
f_0 is the resonant frequency,
c is the speed of light in a vacuum,
ε_r is the permittivity of the substrate.

3.4. RDRA modification

A dielectric resonator with a relative permittivity of 15 was used as the initial RDRA. To improve its bandwidth, selected portions of the resonator centre were removed to produce the H-shaped geometry shown in Figure 4(b).

This modification created a central air-filled region with a relative permittivity of 1 (εr = 1). The removal can be defined by two cut dimensions, which are the horizontal cut width Wdrcut = 6 mm and the vertical cut length Ldrcut = 5 mm.

These two cuts together form the characteristic H-shaped profile. This modification altered the distribution of electromagnetic energy within the resonator and effectively reduced the overall effective permittivity (εeff) of the structure.

$$\varepsilon_{eff} = \frac{h_{eff}}{\frac{h_{dra}}{\varepsilon_{dra}} + \frac{h_{sub}}{\varepsilon_{sub}} + \frac{h_{air}}{\varepsilon_{air}}} \quad (9)$$

$$Q = 2\omega \frac{Stored\ Energy}{Radiated\ Power} \ \alpha\ 2\omega(\varepsilon_{eff})^p (\frac{Volume}{Surface})^s \quad (10)$$

$$BW = \frac{f}{Q} \quad (11)$$

With the modified geometry and (9), the effective permittivity was drastically reduced to 1.88 from 15. This indicates that introducing an air gap leads to a reduction in the effective permittivity (εeff).

As shown in (10), the quality factor Q is proportional to the value of ε_eff, and a lower value of effective permittivity will lead to a lower value of the Q-factor.

A low Q-factor means less stored energy and high electromagnetic coupling inside the resonator, which will ultimately help to widen the impedance bandwidth.

The general expression for the Q-factor, derived from the basic geometric parameters of the antenna, is given in [19], where P > S ≥ 1, and ω is the resonant angular frequency.

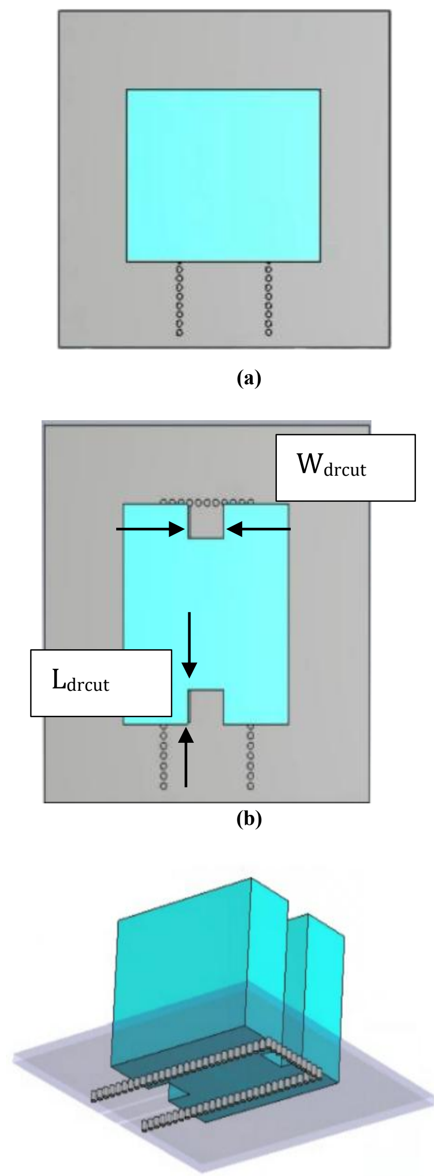

(a)

(b)

(c)

Fig. 4 Geometry of the dielectric resonator structures, (a) Front view of the conventional RDRA, (b) Front view of the modified H-DRA with cut dimension, and (c) Perspective view of the overall H-DRA configuration.

This relationship is further validated by (11), which shows that the antenna Bandwidth (BW) is inversely proportional to the Q-factor. Therefore, decreasing εeff and the corresponding Q-value directly enhances the overall bandwidth performance of the antenna.

An expression illustrating the relationship between the Bandwidth (BW) and the radiation Q-factor (Q) of the DRA is given as follows [20, 21]. The H-DRA also exhibits a lower volume-to-surface ratio compared to the conventional RDRA (2.85 vs. 4.74), as shown in Table 4.

Table 3. Comparison of the volume-to-surface ratio between the single-element RDRA and H-DRA of basic RDRA

Antenna Types /Parameter	RDRA	H-DRA
ε_r	15	15 & 1
ε_{eff}	-	1.88
S (mm^2)	4912	7456
Volume (mm^3)	23296	21216
V/S ratio	4.74	2.85

4. Results and Discussion

4.1. Comparative Study of Three Different Planar Feeding Lines (ML, APC, and CPW)

The simulated return loss (S11) characteristics of the RDRA using the three planar feeding techniques are presented in Figure 5, and all the output performance results are summarized in Table 5. This comparative study aims to identify the optimal feeding configuration for the proposed RDRA antenna. Three planar feeds were implemented for the single RDRA structure, namely ML, APC, and CPW, as illustrated in Figure 2. To ensure a fair comparison, the RDRA height was kept constant at d = 22 mm for all cases so that the antenna operated under the same dominant (fundamental) TE mode. With the mode-defining height fixed, the lateral dimensions were allowed to vary slightly to improve resonance and impedance matching.

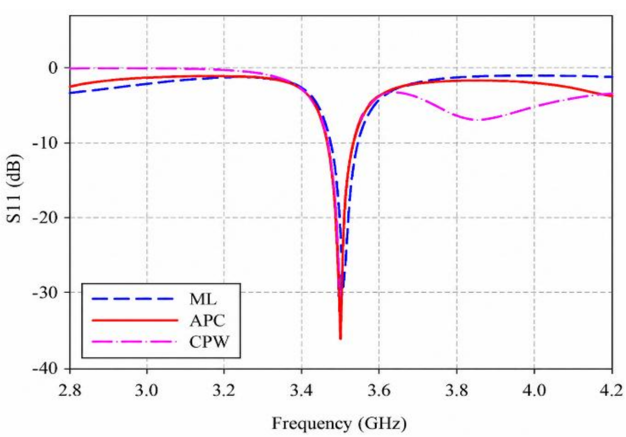

Fig. 3 Simulated S_{11} responses of the different planar feeding configurations

Table 4. Performance comparison of the three different planar feeding configurations

Output Performance	Three Planar Feeding Lines		
	ML	APC	CPW
S11 (dB)	-27.53	-35.72	-34.66
Gain (dBi)	4.88	3.04	3.92
Bandwidth (MHz)	67	63	63
Dimension width x length of DRA, (a x b) (mm)	20 x 21	24 x 21	20 x 20
Dimension height of DRA, d (mm)	22	22	22

The S_{11} curves showed clear differences in impedance matching among the three feeding configurations. The APC-fed RDRA provided the strongest matching with a minimum S11 of −35.72 dB, followed by the CPW fed and ML fed configurations at −34.66 dB and −27.53 dB, respectively. In terms of gain, the ML fed RDRA achieved the highest gain of 4.88 dBi, followed by the CPW fed configuration at 3.92 dBi, whereas the APC fed design yielded the lowest gain of 3.04 dBi. The −10 dB impedance bandwidth was comparable across the designs, with CPW and APC both achieving 63 MHz, while ML provided a slightly wider bandwidth of 67 MHz. Although the computed −10 dB impedance bandwidths were comparable, the CPW fed RDRA exhibited an additional S11 reduction in the upper frequency region, indicating potential for further bandwidth enhancement in subsequent design stages.

In addition, the physical dimensions varied with the feeding structure, as summarized in Table 5. The APC fed design required a larger dimension (24 × 21 mm²), whereas the ML and CPW configurations remained more compact at 20 × 21 mm² and 20 × 20 mm², respectively, while maintaining the same height. Although the ML fed RDRA was comparable in size at this stage, integrating an SIW section is expected to increase the overall antenna length because an additional transition, such as a taper, is typically needed to interface the microstrip feed with the SIW. Therefore, CPW was selected as the baseline feeding scheme to preserve compactness while maintaining good matching performance. Meanwhile, the relatively lower gain was addressed in the next stage through SIW based gain enhancement. The following section further analyzes the CPW fed configuration prior to SIW integration to justify its suitability as the baseline design.

4.2. Performance Analysis of the CPW based Feeding Configurations

As summarized in Table 6, the addition of the slot produced only a slight increase in impedance bandwidth, whereas substantial improvements in impedance bandwidth, gain, and impedance matching were achieved after the SIW structure was integrated with the CPW-slot feeding configuration. The CPW only and CPW slot configurations produced S11 values of −34.66 and −33.91 dB, respectively. Following SIW integration, a deeper S11 response of −39.95 dB was obtained, indicating improved impedance matching.

A substantial improvement was also observed in the gain and impedance bandwidth after SIW integration. The CPW only configuration achieved a gain of 3.92 dBi and a bandwidth of 63 MHz. The addition of the slot slightly broadened the bandwidth to 72 MHz, although the gain decreased marginally to 3.78 dBi. After the SIW structure was integrated, the gain increased to 9.30 dBi, and the impedance bandwidth expanded to 371 MHz. Therefore, the principal performance enhancement was attributed primarily to SIW integration rather than solely to the addition of th slot.

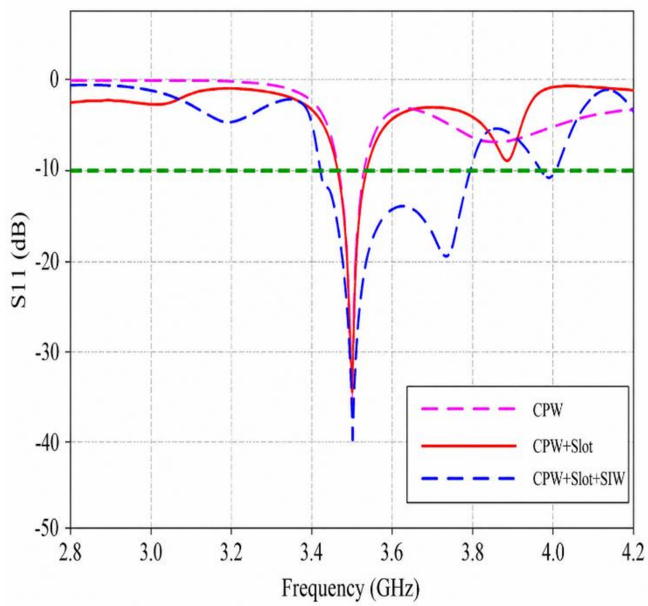

Fig. 6 Simulated S_{11} response of the CPW based feeding configurations

Table 6. Performance comparison of the CPW based feeding configurations

Output Performance	CPW Feeding Configuration		
	CPW	CPW + Slot	CPW + Slot + SIW
S11 (dB)	-34.66	-33.91	-39.95
Gain (dBi)	3.92	3.78	9.3
Bandwidth (MHz)	63	72	371

As illustrated in Figure 7, the SIW structure confines the surface current more effectively around the coupling region beneath the dielectric resonator. Compared with the conventional CPW slot RDRA, the stronger current concentration indicates improved electromagnetic coupling and more effective power transfer from the feeding structure to the resonator.

The SIW structure also limits field leakage from the feeding region, thereby contributing to the higher gain and broader impedance bandwidth reported in Table 6. Compared with the previously reported single-element DRA designs summarized in Table 1, the proposed CPW-slot-SIW RDRA provides competitive gain while retaining a relatively simple single-element configuration.

Nevertheless, its impedance bandwidth remains approximately 10.3% and is narrower than that of several reported wideband designs. Therefore, SIW integration improves the overall antenna performance but does not completely overcome the gain–bandwidth trade-off of the conventional RDRA.

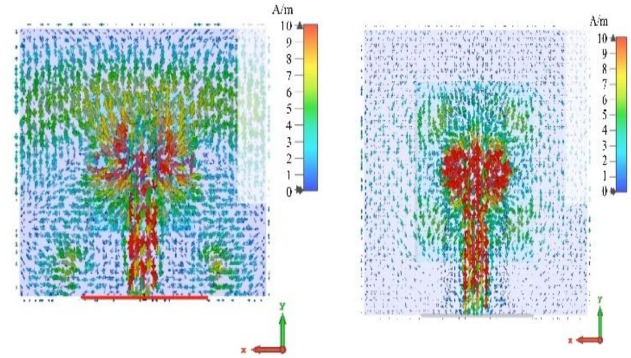

(a) Conventional CPW-slot RDRA (b) Proposed CP-SIW RDRA

Fig. 7 Simulated bottom-view surface current distributions of, (a) The optimized CPW slot fed RDRA without SIW, and (b) The proposed CPW-SIW integrated RDRA, illustrating the improved surface current confinement around the coupling region after SIW integration.

From the far-field radiation patterns shown in Figure 8, the CPW slot SIW configuration produces a directional main lobe with suppressed back radiation and well-controlled side lobes in both principal planes. These characteristics indicate that the SIW structure effectively confines the electromagnetic fields and directs more radiated power towards the main radiation direction. Together with the improved impedance matching, gain, and bandwidth reported in Table 6, these results confirm the suitability of the CPW-slot-SIW configuration as the optimized excitation structure. Nevertheless, further bandwidth enhancement is required to reduce the remaining gain–bandwidth trade-off. Therefore, the following section investigates geometrical modification of the dielectric resonator to broaden the impedance bandwidth while maintaining the gain enhancement achieved through SIW integration.

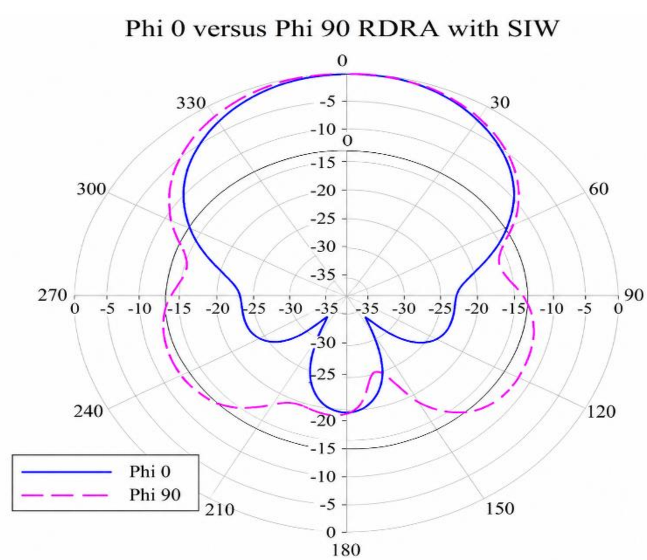

Fig. 8 Radiation pattern of a single RDRA with a CPW slot and SIW integration

4.3. Performance Comparison between the Rectangular and H-shaped DR

The conventional RDRA was modified by removing selected dielectric sections to produce an H-shaped resonator. Both configurations employed an identical CPW–SIW feeding mechanism and were optimized at 3.5 GHz to ensure a consistent comparison. Figure 9 presents the simulated reflection coefficients of the two designs. The H-DRA achieves a reflection coefficient lower than −40 dB at the target frequency, demonstrating effective impedance matching. In addition, the −10 dB impedance bandwidth improves from 10.3% for the original RDRA to 13.9% after the H-shaped modification, as reported in Table 7.

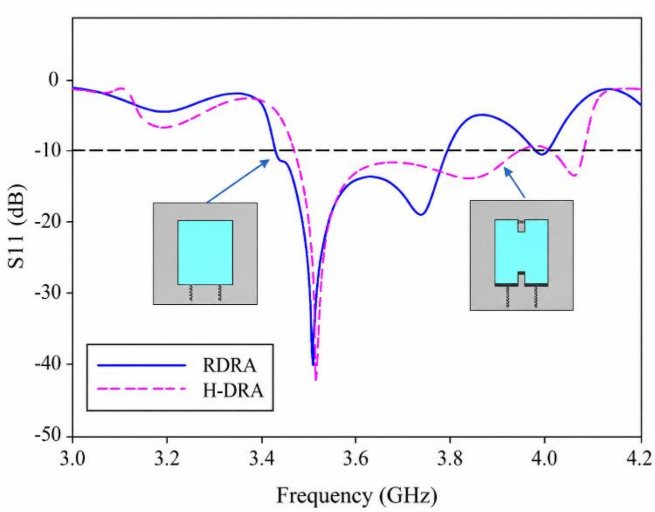

Fig. 9 Simulated S_{11} responses of the conventional RDRA and modified H-DRA resonator shapes

Table 5. Summary of the simulated results of antenna performance

Antenna Types	f_0 (GHz)	Bandwidth (%)	Gain (dBi)	Efficiency (%)
RDRA	3.5	10.3	9.3	98.6
H-DRA	3.5	13.9	9.14	98

The bandwidth enhancement can be explained by the theoretical relationships presented in Section 3.4. The air regions introduced by the H-shaped modification reduce the effective permittivity of the resonator, as described by (9). According to the proportional relationship in (10), the reduction in effective permittivity, together with the lower volume-to-surface ratio of the H-DRA, reduces the resonator quality factor.

Since the impedance bandwidth is inversely proportional to the quality factor, as expressed in (11), the lower Q-factor produces a wider operating bandwidth. This theoretical mechanism is consistent with Figure 9 and Table 7, where the impedance bandwidth increases from 10.3% to 13.9%, representing an approximately 35.0% relative improvement, while the peak gain decreases only marginally from 9.30 to 9.14 dBi. Therefore, the H-shaped air regions broaden the impedance bandwidth without materially compromising the gain enhancement achieved through the CPW-slot-SIW feeding structure.

At the simulation stage, the proposed H-DRA also provides a competitive gain-bandwidth balance relative to the representative SIW integrated DRA techniques listed in Table 1. The stacked SIW-DRA, SIW-fed parasitic DRA array, and shorting via/DGS designs reported fractional bandwidths of 4.64%, 8.9%, and 9.0%, respectively, compared with 13.9% for the proposed H-DRA. Although the fractal and perforated SIW-DRA designs achieved wider bandwidths of 19.5% and 18.5%, their gains were 5.96 and 8.6 dBi, respectively, whereas the proposed H-DRA maintains 9.14 dBi. Although the proposed H-DRA does not achieve the highest individual gain or bandwidth among all the designs listed in Table 1, it provides a favourable balance between these two performance parameters. Unlike stacked or parasitic element techniques, the present approach introduces air regions directly within a single dielectric resonator, thereby reducing the effective permittivity and Q-factor without adding another resonator or external matching element.

Despite the bandwidth enhancement, the H-DRA maintains a high simulated peak gain of 9.14 dBi and a radiation efficiency of approximately 98%. As shown in Figure 10, the E-plane pattern has a well-defined main lobe, indicating that the H-shaped modification preserves directional radiation. The H-plane pattern is less symmetrical but retains a distinct main lobe with moderate sidelobes. The high radiation efficiency indicates that the geometrical modification does not introduce substantial additional dielectric or conductor losses; however, efficiency alone is not evidence of a low resonator Q-factor. The simulated gain and efficiency across the operating frequency range are further presented in Figure 11.

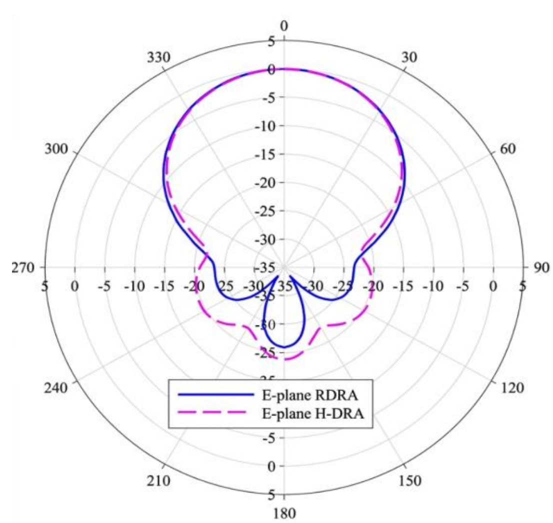

(a)

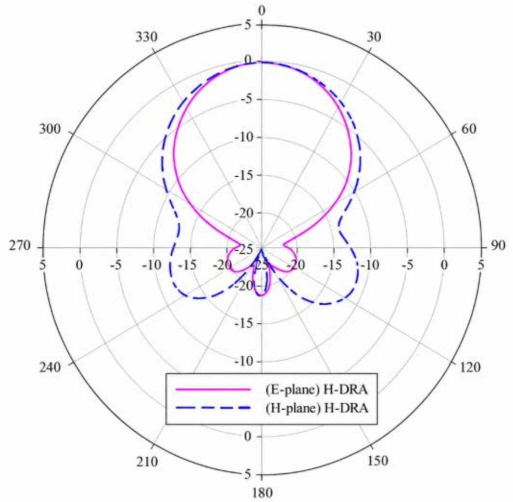

(b)

Fig. 10 Radiation pattern comparison, (a) RDRA versus H-DRA in the E-plane, and (b) E-plane versus H-plane patterns of the H-DRA.

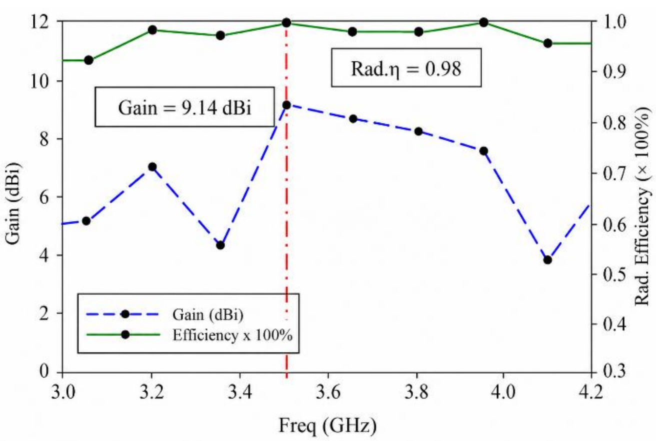

Fig. 11 Simulated gain and efficiency versus frequency of the H-DRA

Overall, the H-shaped modification broadens the impedance bandwidth from 10.3% to 13.9%, while the antenna gain decreases only marginally from 9.30 to 9.14 dBi. The high radiation efficiency and directional radiation characteristics are also maintained. Therefore, compared with the conventional RDRA, the proposed H-DRA provides a more favourable gain–bandwidth balance for Sub 6 GHz operation.

4.4. Experimental Validation

An experimental prototype of the proposed H-DRA was built to validate the simulated results. The fabricated SIW–DRA structure is shown in Figure 12, where the SIW structure and CPW slot feeding network before the ceramic H-shaped DR mounting are depicted in Figure 12(a), the completed prototype (with the ceramic H-shaped DR mounted on the top) is shown in Figure 12(b), and the back view of the completed prototype is shown in Figure 12(c). While performing the verification of design dimensions, the fabricated dimensions were close to the simulated dimensions.

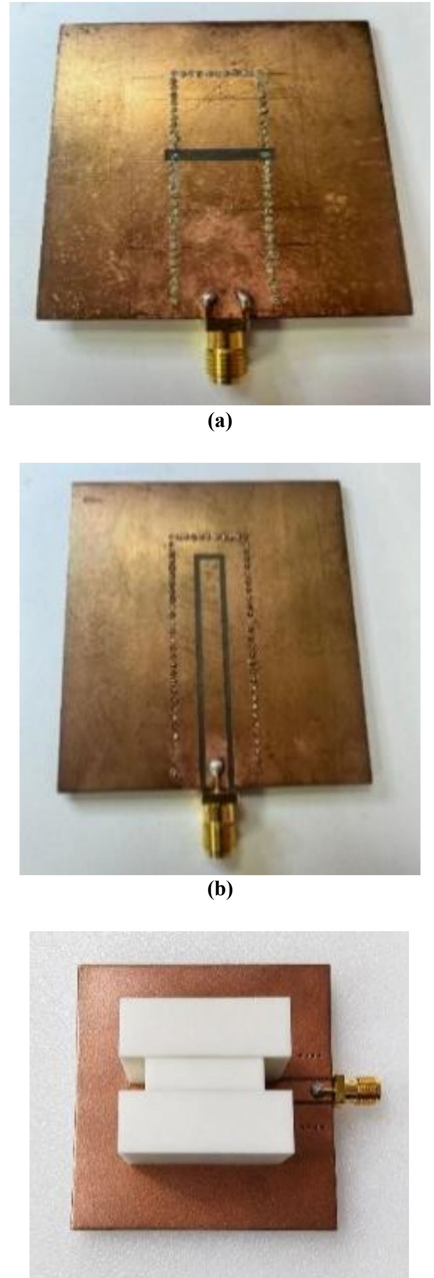

(a)

(b)

(c)

Fig. 12 (a) Front view of the fabricated SIW DRA structure before attaching the ceramic dielectric resonator, (b) Back view and (c) Front view of the fabricated SIW DRA structure after attaching the ceramic dielectric resonator.

Figure 13 shows the S-parameter measurement setup. A Keysight Vector Network Analyzer (VNA) was used to measure the return loss (S11) of the antenna. Before the measurement process, a standard SOLT (Short Open Load Through) calibration was conducted by applying the calibration kit with the aim of removing the effects of cable and connector losses. Then, the Antenna Under Test (AUT) was placed on a non-conductive platform to minimize reflection errors in the measurement process.

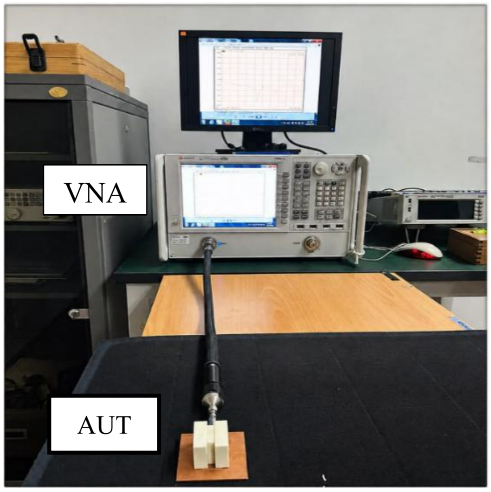

Fig. 13 S-parameter measurement equipment

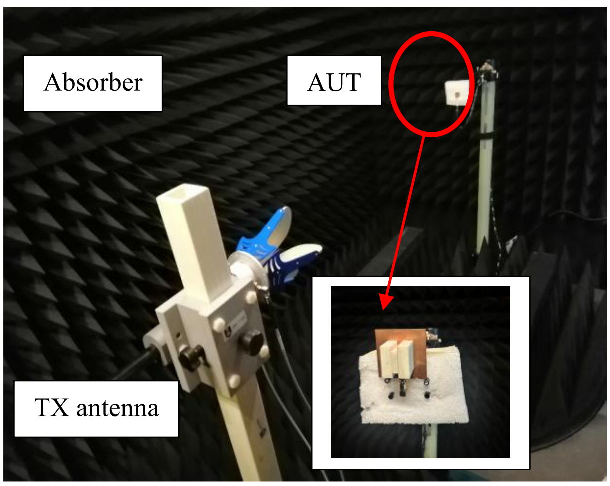

Fig. 14 OTA 500 anechoic chamber measurement

Subsequently, the radiation characteristics were evaluated inside an OTA-500 anechoic chamber, as shown in Figure 14. The chamber was fully lined with RF absorbers to suppress unwanted reflections. A standard gain horn antenna was used as the Transmitting (TX) antenna, and the AUT was mounted on a motorized rotational platform to capture radiation patterns over both θ and ϕ directions. The rotation mechanism supports a full 360° sweep in the horizontal plane and up to 165° in the vertical plane, enabling accurate characterization of the antenna's gain and radiation characteristics.

Figure 15 shows the measured and simulated S11 responses. For both cases, the antenna met the impedance matching requirement of S11 < -10 dB within the considered frequency range, which indicates good impedance matching performance within the operating frequency band. The two results show a small difference in resonance frequencies. The simulated antenna showed a minimum return loss of S11 = -44.59 dB at 3.50 GHz, while the measured prototype resonated at 3.56 GHz, with a minimum return loss of S11 = -49.94 dB. A slight upward shift in the resonant frequency of approximately 60 MHz is observed in the measured result. Moreover, the simulated result showed a –10 dB impedance bandwidth of 0.5195 GHz from 3.47 GHz to 3.99 GHz, while the measured result showed 0.992 GHz from 3.087 GHz to 4.08 GHz.

The results of measured antenna performance are summarized in Table 8. This indicates that the measured impedance bandwidth is more than twice the simulated bandwidth.

The small mismatch between the simulated and measured performances is primarily due to fabrication tolerances, a minor mismatch in the value of the dielectric constant of the ceramic material, manual drilling misalignment of the SIW vias, and minor inaccuracies in the assembly process when placing the resonator.

However, both curves display a similar overall trend, showing that the fabricated prototype is a good approximation of the simulated impedance pattern of the prototype.

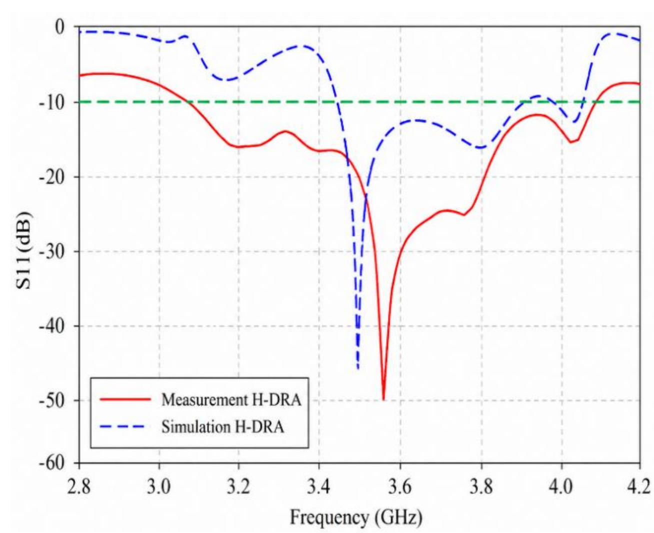

Fig. 15 Comparison of the simulated and measured S_{11} responses of the H-DRA antenna

Table 8. Summary of measured performance of the H-DRA antenna

Antenna Types	f_0 (GHz)	Bandwidth (GHz)	Bandwidth (%)	Gain (dBi)
H-DRA	3.56	0.992	27.7	8.29

The general behavior of the measured results and simulated response in terms of resonance behavior and impedance matching is in good agreement with each other.

The results obtained confirm the validity of the proposed feeding technique (CPW slot SIW) and the resonator shape (H-shaped) to obtain the wide impedance bandwidth for practical 5G applications.

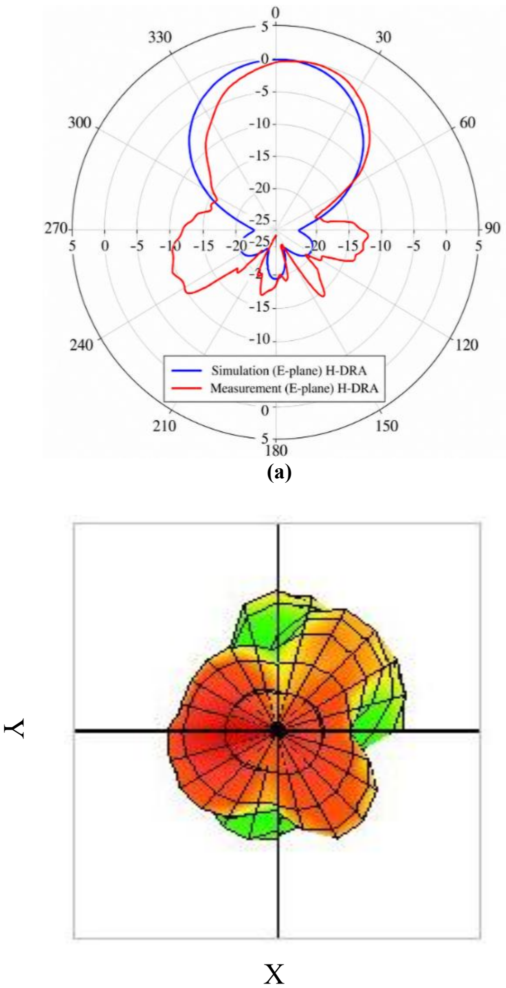

(a)

(b)

Fig. 16 Simulated and measured radiation characteristics of the single H-DRA antenna, (a) Simulated and measured E-plane radiation patterns, and (b) Measured 3D radiation pattern.

5. Conclusion

A high-gain wideband H-DRA is successfully developed and experimentally validated using a CP-SIW feeding configuration for Sub-6 GHz 5G applications. The integration of SIW within the CPW-slot feeding structure, combined with the modified H-shaped resonator, effectively improves the impedance bandwidth while maintaining high gain and stable radiation behavior. This combination of techniques successfully reduces the gain–bandwidth trade-off. According to experimental results, this proposed antenna successfully resonates at 3.56 GHz and has a measured impedance bandwidth of 0.992 GHz (27.7%). The antenna also shows minimal back radiation and a peak gain of approximately 8.29 dBi. The radiation pattern shows a slight beam shift of about 10°, but these measured results are still in good agreement with the simulated performance. The only minor differences are due to fabrication tolerances and experimental uncertainties. Overall, the proposed CPW slot SIW fed H-DRA provides a compact and efficient antenna solution capable of meeting the bandwidth and gain requirements of Sub 6 GHz 5G wireless communication systems. Furthermore, the results indicate that the combined implementation of CP-SIW feeding and an H-shaped dielectric resonator provides an effective approach for improving bandwidth while maintaining high gain performance. This design strategy may serve as a useful reference for future SIW-DRA development targeting Sub 6 GHz 5G wireless communication systems.

Conflicts of Interest

The authors declare that there is no conflict of interest regarding the publication of the paper.

Funding statement

This work was financially supported by Universiti Teknologi MARA (UiTM) under the incentives of 'Pembayaran Yuran Prosiding Berindeks (PYPB)'.

Acknowledgments

The authors would like to express their sincere appreciation to the members of Universiti Teknologi MARA (UiTM), the Antenna Research Group (ARC), the Wireless Telecommunication Group, ARI, the Wireless Communication Center (WCC), Universiti Teknologi Malaysia (UiTM), and the Center for Intelligent Network TM Research & Development (TM R&D) for their valuable guidance and support throughout this research.

References

[1] Jin Shi et al., "Endfire Substrate Integrated Dielectric Resonator Antenna with Dual-Beam Radiation for Millimeter-Wave Application," *IEEE Antennas and Wireless Propagation Letters*, vol. 23, no. 5, pp. 1523-1527, 2024. [CrossRef] [Google Scholar] [Publisher Link]

[2] Emmanuel K. Chemweno, Pradeep Kumar, and Thomas J.O. Afullo, "Substrate Integrated Waveguide-Dielectric Resonator Antenna for Future Wireless Communication," *SAIEE Africa Research Journal*, vol. 113, no. 3, pp. 119-128, 2022. [CrossRef] [Google Scholar] [Publisher Link]

[3] Sidhartha Kumar Sahu et al., "High Gain SIW-Fed Notched Spherical-Frustum Shaped Stacked DRA for B5G Application," *2025 19th European Conference on Antennas and Propagation*, Stockholm, Sweden, pp. 1-5, 2025. [CrossRef] [Google Scholar] [Publisher Link]

[4] Hui Tang, Xiaowei Deng, and Jin Shi, "Wideband Substrate Integrated Differential Dual-Polarized Dielectric Resonator Antenna," *IEEE Antennas and Wireless Propagation Letters*, vol. 21, no. 1, pp. 203-207, 2022. [CrossRef] [Google Scholar] [Publisher Link]

[5] Emmanuel K. Chemweno, Pradeep Kumar, and Thomas J.O. Afullo, "Bandwidth Enhancement of a Substrate Integrated Waveguide Dielectric Resonator Antenna using Metallic Shorting Vias," *2022 International Conference on Electromagnetics in Advanced Applications*, Cape Town, South Africa, pp. 302-305, 2022. [CrossRef] [Google Scholar] [Publisher Link]

[6] Wei Luo et al., "A Novel Wideband Fractal Rectangular Dielectric Resonator Antenna with Improved Radiation Performance," *AEU-International Journal of Electronics and Communications*, vol. 142, 2021. [CrossRef] [Google Scholar] [Publisher Link]

[7] E.K. Chemweno, P. Kumar, and T.J.O. Afullo, "Design of High-Gain Wideband Substrate Integrated Waveguide Dielectric Resonator Antenna for D-Band Applications," *Optik*, vol. 272, 2023. [CrossRef] [Google Scholar] [Publisher Link]

[8] Arshad Hassan et al., "Substrate Integrated Waveguide based Multiband Antenna Array for Midband 5G and IoT Applications," *2024 15th International Conference on Information and Communication Technology Convergence*, Jeju Island, Korea, pp. 2111-2114, 2024. [CrossRef] [Google Scholar] [Publisher Link]

[9] Umesh Chandra Singh, and Rajesh Mishra, "Design of Substrate Integrated Waveguide (SIW) Slot Antenna for Millimeter-wave 5G Application," *2021 International Conference on Industrial Electronics Research and Applications*, New Delhi, India, pp. 1-4, 2021. [CrossRef] [Google Scholar] [Publisher Link]

[10] G. Divya et al., "Encapsulated Tri-Band Terahertz (Thz) Swiveled Dielectric Resonator Antenna (DRA) with Substrate Integrated Waveguide (SIW) and Photonic Band Gap (PBG) Crystal for Gain Enhancement," *Scientific Reports*, vol. 15, no. 1, pp. 1-17, 2025. [CrossRef] [Google Scholar] [Publisher Link]

[11] King Tung Lo, and Hang Wong, "Wideband Millimetre-Wave Dielectric Resonator Antenna Fed by a Wide Aperture," *IEEE Access*, vol. 12, pp. 14521-14531, 2024. [CrossRef] [Google Scholar] [Publisher Link]

[12] Jianxing Li et al., "Wideband Circularly Polarized Substrate Integrated Dielectric Resonator Antenna Array for 5G Millimeter-Wave Applications," *IEEE Antennas and Wireless Propagation Letters*, vol. 23, no. 12, pp. 4378-4382, 2024. [CrossRef] [Google Scholar] [Publisher Link]

[13] Wael Mahmoud Abdel-Wahab et al., "SIW-Integrated Parasitic DRA Array: Analysis, Design, and Measurement," *IEEE Antennas and Wireless Propagation Letters*, vol. 18, no. 1, pp. 69-73, 2019. [CrossRef] [Google Scholar] [Publisher Link]

[14] Ehsan Rahmati, Daniel N. Aloi, and Mohammad S. Sharawi, "60 GHz Perforated Dielectric Resonator Antenna Fed by Substrate Integrated Waveguide," *2023 IEEE International Symposium on Antennas and Propagation and USNC-URSI Radio Science Meeting*, Portland, OR, USA, pp. 1163-1164, 2023. [CrossRef] [Google Scholar] [Publisher Link]

[15] Meshari D. Alanazi, and Salam K. Khamas, "A Compact Dual Band MIMO Dielectric Resonator Antenna with Improved Performance for mm-Wave Applications," *Sensors*, vol. 22, no. 13, pp. 1-15, 2022. [CrossRef] [Google Scholar] [Publisher Link]

[16] Aymen Dheyaa Khaleel et al., "Pattern Reconfigurable Dielectric Resonator Antenna using Multi-Feed Technique for LTE and Wi-Fi Applications," *2018 IEEE 4th International Symposium on Telecommunication Technologies*, Selangor, Malaysia, pp. 1-5, 2018. [CrossRef] [Google Scholar] [Publisher Link]

[17] D. Deslandes, and Ke Wu, "Accurate Modeling, Wave Mechanisms, and Design Considerations of a Substrate Integrated Waveguide," *IEEE Transactions on Microwave Theory and Techniques*, vol. 54, no. 6, pp. 2516-2526, 2006. [CrossRef] [Google Scholar] [Publisher Link]

[18] Bin Feng Zong, Hui Yong Zeng, and Fan Wu, "Field Distributions Analyzed of Substrate Integrate Waveguide (SIW)," *Procedia Computer Science*, vol. 166, pp. 241-247, 2020. [CrossRef] [Google Scholar] [Publisher Link]

[19] Duggirala Venkata Kiran, Dileep Sankaranarayanan, and Biswajeet Mukherjee, "Compact Embedded Dual-Element Rectangular Dielectric Resonator Antenna Combining Sierpinski and Minkowski Fractals," *IEEE Transactions on Components, Packaging and Manufacturing Technology*, vol. 7, no. 5, pp. 786-791, 2017. [CrossRef] [Google Scholar] [Publisher Link]

[20] Hui Chu et al., "Implementation of Synthetic Material in Dielectric Resonator-based Filtering Antennas," *IEEE Transactions on Antennas and Propagation*, vol. 66, no. 7, pp. 3690-3695, 2018. [CrossRef] [Google Scholar] [Publisher Link]

[21] Sriparna Bhattacharya (Mitra), and Sekhar Chandra Ray, "Broadbanding and Multi-Frequency in Dielectric Resonator Antennas: A Comprehensive Review," *International Journal of Microwave and Wireless Technologies*, vol. 15, no. 4, pp. 709-725, 2023. [CrossRef] [Google Scholar] [Publisher Link]